ACS APPLIED MATERIALS & INTERFACES

Research Article

www.acsami.org

Efficient Coupling of Optical Energy for Rapid Catalyzed Nanomaterial Growth: High-Quality Carbon Nanotube Synthesis at Low Substrate Temperatures

Muhammad Ahmad, Jose V. Anguita, Vlad Stolojan, J. David Carey, and S. Ravi P. Silva*

Advanced Technology Institute, University of Surrey, Guildford GU2 7XH, United Kingdom

ABSTRACT: The synthesis of high-quality nanomaterials depends on the efficiency of the catalyst and the growth temperature. To produce high-quality material, high-growth temperatures (often up to 1000 °C) are regularly required and this can limit possible applications, especially where temperature sensitive substrates or tight thermal budgets are present. In this study, we show that high-quality catalyzed nanomaterial growth at low substrate temperatures is possible by efficient coupling of energy directly into the catalyst particles by an optical method. We demonstrate that using this photothermal-based chemical vapor deposition method that rapid growth (under 4 min, which includes catalyst pretreatment time) of high-density carbon nanotubes can be grown at substrate temperatures as low as 415 °C with proper catalyst heat treatment. The growth process results in nanotubes that are high quality, as judged by a range of structural, Raman, and electrical characterization techniques, and are compatible with the requirements for interconnect technology.

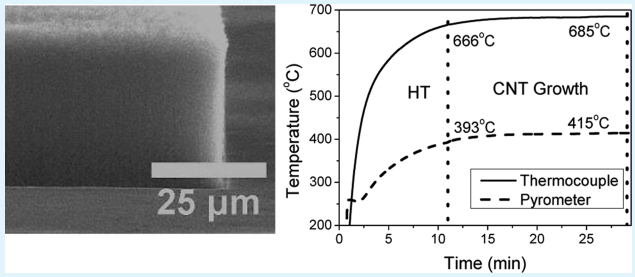

KEYWORDS: *catalyzed nanomaterial growth, photothermal chemical vapor deposition, low temperature growth, carbon nanotubes, interconnects*

High-aspect-ratio nanomaterials, such as carbon nanotubes (CNTs), have potential applications for use in integrated circuit interconnects,[1−3] nanoprobes,[4] large area displays,[5] and a variety of electronic devices.[6,7] One application area that could naturally exploit the high aspect ratio of the CNTs, coupled with their excellent electrical properties, is in the area of electrical interconnects. The international technology roadmap for semiconductors (ITRS) emphasizes the need of new materials for interconnect applications to maintain the pace of technology.[8] The advantageous properties of CNTs, including ballistic conduction,[9] high current carrying capacity,[10] high thermal conductivity,[11] as well as high tensile strength[12] makes vertically grown nanotubes in vias for vertical interconnect access highly attractive. A key requirement for the use of CNTs as interconnects is growth at CMOS compatible temperatures without compromising structural and electrical quality, hence understanding and developing nanotube growth at low temperatures is important.

The quality and length of CNTs grown using catalyzed chemical vapor deposition (CVD) depends on the growth temperature. Selective growth of multiwall carbon nanotubes (MWCNTs) in vias has been previously demonstrated using conventional CVD or plasma-assisted CVD methods in the temperature range of 390−700 °C.[1,13,14] However, CNTs growth in the lower temperature range of 390−550 °C tends to result in a higher concentration of structural defects,[13,15] which in turn introduce more scattering centers. In addition, the growth rate of nanotubes on metal (conductive) substrates in the lower temperature range is typically very low (0.05−0.16 μm/min).[16] Apart from the growth time, pretreatment of the catalyst prior to growth takes additional time, ranging from 10 to 60 min.[17−19] Here, we demonstrate how efficient optical coupling of energy at the growth front of properly engineered catalyst surface can produce high-quality CNTs with high growth rates, in excess of 3 μm/min, and at CMOS-compatible temperatures for direct integration as interconnects. We further explore the growth initiation as a function of catalyst heat-treatment (HT) time and temperature and has led us to propose a photothermal rapid growth process (PT-RGP) where the total process time (catalyst preheating and growth time) to grow CNTs of length in excess of a micrometer is less than 4 min. The principle of using an optical source where the energy is efficiently coupled to the catalyst is not just limited to nanotubes and can be applied to other systems for engineered catalyzed growth using chemical vapor deposition-based methods. As such a broad aim understanding the factors associated with the thermal treatment of the catalyst and associated nanomaterial growth becomes a key question and is the subject of this study.

RESULTS AND DISCUSSION

Figure 1 contains SEM micrographs of CNTs grown for 15 s and 2, 10, and 20 min after 10 min of heat treatment. Growth

Received: February 8, 2013
Accepted: April 15, 2013
Published: April 15, 2013

   dx.doi.org/10.1021/am400542u | ACS Appl. Mater. Interfaces 2013, 5, 3861−3866

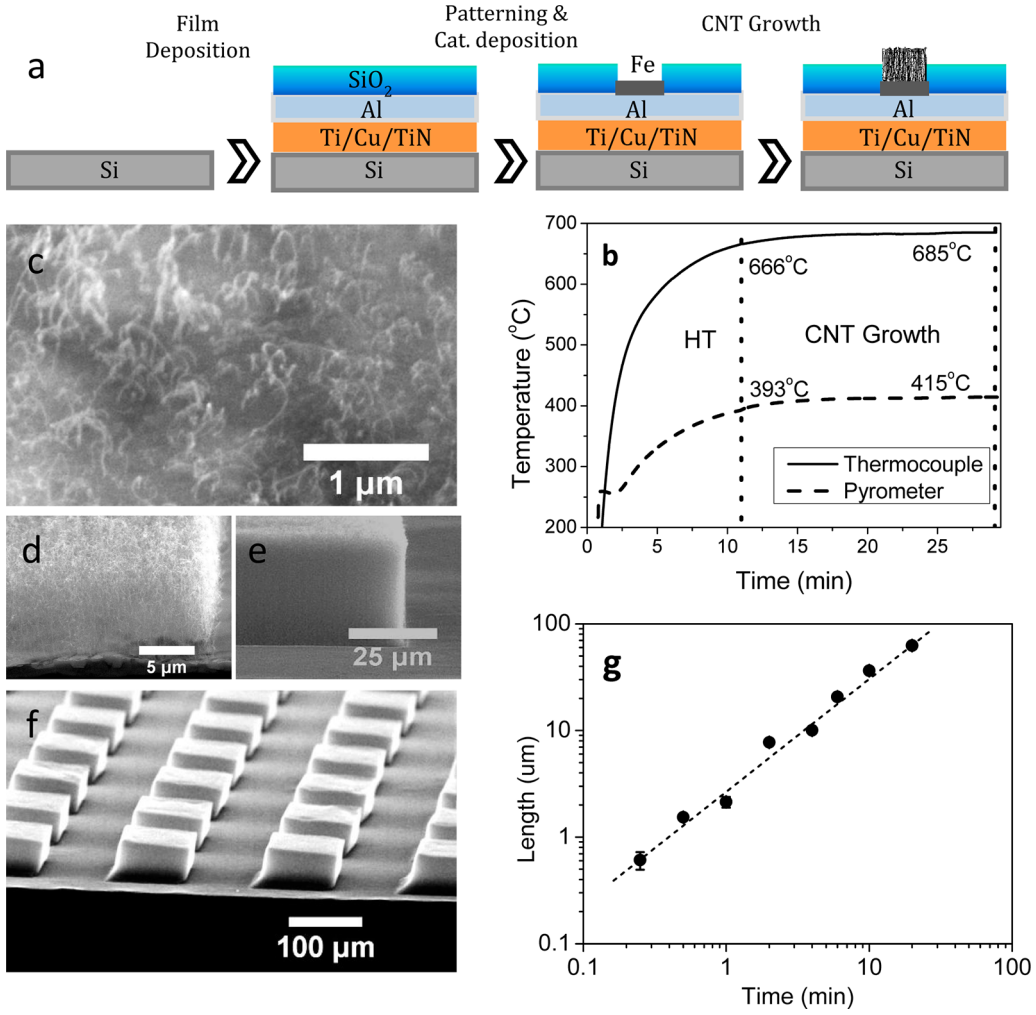

Figure 1. (a) Process schematic for the CNT growth in via contacts. (b) Temperature profiles for 20 min CNT growth after 10 min heat-treatment, recorded by the pyrometer at the bottom and thermocouple at the top surface of the sample, under 2 Torr pressure (100 sccm H_2 and 10 sccm C_2H_2) and 40% (~ 3.2 kW) electrical power supplied to the lamps. (c-f) SEM images ((c) tilted 45°, (d–f) tilted 75°) for 15 s and 2, 10, and 20 min of CNT growth durations resulted in about 0.5, 8, 36, and 63 μm long vertically aligned CNTs, respectively. (g) The plot shows that the growth is linear at a rate of ~3.2 μm/min.

starts immediately after introducing C_2H_2 into the chamber, as can be observed in Figure 1c where after only 15 s, CNTs of lengths in excess of 500 nm are observed. The length of the CNTs increases linearly with respect to the growth time (Figure 1g) and CNTs of about 63 μm in length were achieved after 20 min growth (Figure 1f). The as-grown CNTs are vertically aligned, dense (~1×10^9 cm^{-2}) and growth occurred only in the predefined areas. The presence of an encapsulated catalyst particle at the tip of the CNTs confirms that they grow via a tip-growth mechanism. The growth rate of CNTs is calculated as 3.2 μm/min, which is a higher value compared with other reports of CNTs grown on metal surfaces (0.05–1.3 μm/min);[16] CNT growth on metal surfaces is a prerequisite to their use as interconnects. The high growth rate using the PTCVD system is attributed to the efficient energy delivery to the catalyst in the top-down heating scheme.[16] The use of an Al layer under the Fe catalyst has a marked effect on the increased growth rate and the vertical alignment of the CNTs, as Al directly affects the agglomeration process of the Fe catalyst.[17,20]

The Raman spectra (using 514 nm wavelength) of the as-grown CNTs show well-defined first order and second order features (Figure 2a). The most intense features in the Raman spectra are the D band around 1342 cm^{-1}, the G band around 1578 cm^{-1} and the 2D band around 2690 cm^{-1}. The D band is attributed to the disorder induced A_{1g} Raman mode,[21] and the G band corresponds to the Raman-active E_{2g} vibration of neighboring sp^2 carbon atoms[22] its intensity represents the degree of graphitization in the material. The intensity ratio of the D band to the G band (I_D/I_G) is used as a measure of structural quality of graphite-like materials[23] whereas the 2D band is the overtone of the D band but independent of crystalline defects.[24] The intensity of the 2D band increases and that of the D band decreases with increasing graphitization in the material,[25,26] therefore, their intensity ratio, I_D/I_{2D}, is another metric of CNT quality; this is also supported by the similar trends observed in panels b and c in Figure 2. The low I_D/I_G ratios (0.67–0.44) and the presence of fully developed 2D bands in the Raman spectra given in Figure 2(a) indicate the high quality of as-grown CNTs, comparable with those grown by the arc-discharge method.[27,28] The measured growth rate in the present work has improved to 3.2 μm/min from 1.3 μm/min (when compared to our previous study, ref 16) and there is a large improvement in the quality of CNTs grown in the current work as evident from the TEM and Raman

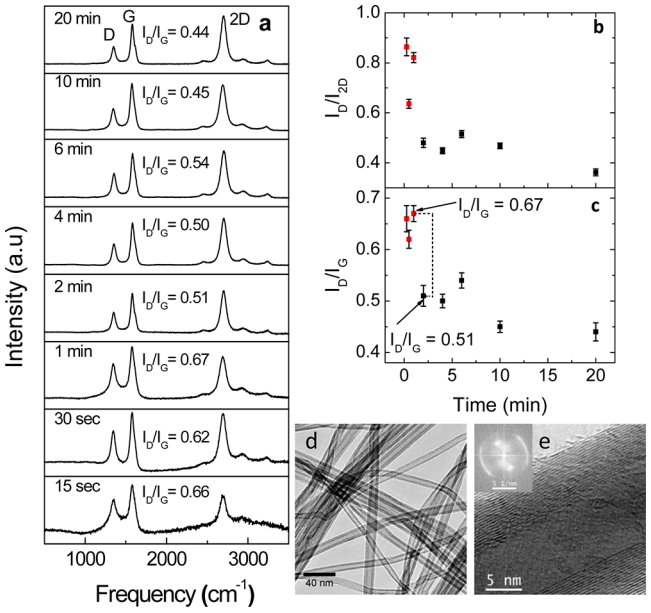

Figure 2. (a) Raman spectra (514 nm laser wavelength) of as grown CNTs for different growth times showing distinct and sharp first order as well as second order peaks. (b, c) Variation of the I_D/I_G and I_D/I_{2D} are plotted against the CNT growth durations. (d) TEM image shows high-quality CNTs, maintaining long-range orders in them. (e) HRTEM images show that the walls of CNTs are well-graphitized. Inset: FFT of e reveals good long-range ordering.

spectroscopy. For example, the I_D/I_G ratio has reduced to 0.44 in the current work whereas it was 1.3 in the previous study. The improvement in the quality and growth rate of the CNTs may both be attributed to the increased bulk temperatures of 393−415 °C (in the previous study it was 370 °C) and different layer structures. In ref 16, the CNT growth was carried out on SiO_2 on Si substrate using Fe/Ti as catalyst whereas in the present work it is on metallic structure of Fe on Al on Ti/Cu/TiN substrate. This should be noted as CNT growth on metallic vs nonmetallic samples will be very different.

The I_D/I_G ratio decreases from 0.66 to 0.44 (Figure 2a) as the CNT growth duration increases from 15 s to 20 min, whereas the corresponding increase in the temperature is only 19 °C (from 666 to 685 °C, see Figure 1b). Yun Tack et al. reported a decrease in the I_D/I_G value from 0.74 to 0.45 as the temperature is increased 300 °C (from 800 to 1100 °C).[29] Campose-Delgado et al. performed heat-treatment on as-produced graphene nanoribbons in the temperature range of 1000−2800 °C and reported a decrease in the I_D/I_G values from ∼1.25 to 0.5 as the temperature increases from 1000 to 2000 °C.[26] Similarly, a decrease in I_D/I_G value from 1.2 to 0.8 corresponding to 750−950 °C CNT growth temperature is reported.[30] In view of these reports, it is clear that although the I_D/I_G values decrease with increasing growth temperature, the I_D/I_G ratio is not highly sensitive to the temperature whereby only a 19 °C increase can cause a decrease from 0.66 to 0.44. Analysis of the data in Figure 2c reveals that the values of I_D/I_G for CNTs grown for short times (up to 1 min) are similar to each other (0.62−0.67) and then there is a step decrease to 0.51 for 2 min CNT growth time, although the temperature remains almost constant.

To explain the step decrease in the I_D/I_G ratio, it is worth recalling the absorption properties of the CNT forest. Mizuno et al. have shown that a forest of single wall CNTs behaves like a blackbody over a very wide spectral range (0.2−200 μm) and their emissivity is as high as 0.98−0.99 for a spectral range of 5−12 μm.[31] In PTCVD, the optical energy delivered by the lamps coarsens the catalyst film and increases its temperature. The initial CNT growth and degree of graphitization depends on the surface temperature of the catalyst particles. However, as the CNT forest grows taller, it itself start to absorb optical energy, which is coupled directly at the growth front, resulting in a sharp decrease in the I_D/I_G ratio. As the length of the CNT forest increases further, the energy absorbed increases gradually, leading to improved graphitization and a steady decrease in I_D/I_G values from 0.51 to 0.44. Thus, keeping the substrate temperature below 415 °C in the top-down energy delivery scheme, we have achieved the growth of high quality vertically aligned CNTs, with the structural quality comparable to that achieved at 2000 °C.[26] The obtained I_D/I_G values are some of the lowest reported for CVD-grown CNTs in the literature, with a value consistently below 0.5 for the equilibrium steady-state conditions.

TEM images d and e in Figure 2 for 20 min growth time supports the analysis of the Raman spectra, showing high structural quality of as-grown CNTs. Figure 2d reveals that the CNTs have very clean straight walls with long-range structural order and are hollow. Statistical analysis on over 150 tubes shows that the mean diameter of CNTs is 14 ± 4 nm with an average of 9 ± 4 shells. The HRTEM image in Figure 2e shows that the walls of the CNTs are highly graphitized. The spacing between the walls is about 0.34 nm, which is equal to the interplanar spacing in graphite. The fast-Fourier transform of Figure 2e (inset) shows good long-range order and is similar to the graphitization achieved by heat-treating petroleum pitch (Ashland's Aerocarb 80) in the range of 2000−2730 °C.[32] This is of significant industrial relevance as it demonstrates the growth of high quality MWCNTs in the surface-heating scheme while controlling the substrate bulk temperature below 415 °C. The high quality of the CNTs is a result of the efficient energy delivery to the top surface of the samples, contrary to the conventional hot-wall CVD methods where the energy transfer to the catalyst is through the substrate, damaging the substrate first and reducing the energy at the growth front.

The SEM image in Figure 1c shows that the CNT growth starts readily after 10 min HT. This HT time is already short, as it includes temperature ramping time. To investigate if HT time can be reduced further, we preheated samples for 5, 6, and 7 min and conducted CNT growth for 1 min while keeping the remaining parameters unchanged. No evidence of CNT growth observed for 5 min HT (Figure 3a), with some tubes just being initiated after 6 min HT (Figure 3b), and a good growth of CNTs with length in excess of 1 μm for 7 min HT (Figure 3c). This was cross-checked; after 5 min HT, C_2H_2 was introduced for 2 and 3 min, respectively, while keeping all remaining conditions the same. The results are similar to those in Figure 3a−c, that is, just initiation of CNT growth after 2 min and a good growth after 3 min. This suggests that the growth of CNTs does not start prior to a threshold condition, even if the carbon feedstock is introduced earlier. These results are in agreement with Seidel et al.[33] who found that 5 min HT under 2.5 Torr H_2 pressure at 650 °C is insufficient for the growth of single wall CNTs on an Al/Ni (3 nm/0.2 nm) structure, and instead a 10 min HT produced good results. However, they did not establish the exact CNT growth initiation point in terms of HT time and temperature. Shang et al. claimed an immediate start of CNT growth on Fe/Ti (1 nm/0.5 nm) bilayers, without

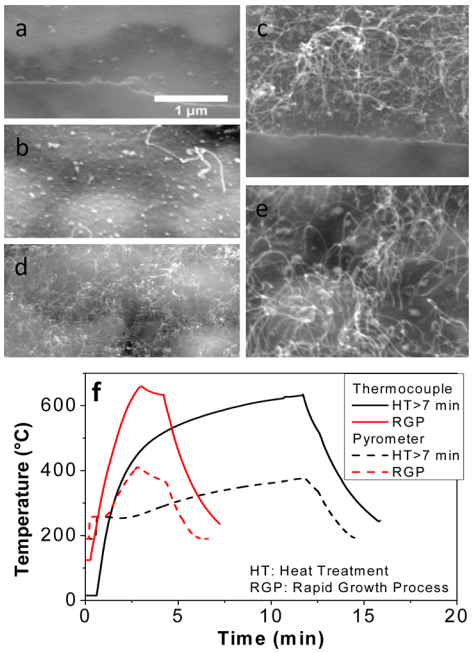

Figure 3. (a) SEM image for 1 min growth after 5 min HT shows no signs of CNT growth; (b) 6 min HT shows initiation of growth and some tubes; (c) 7 min HT shows a good growth of CNTs having lengths >1 μm; (d) SEM image of sample grown for HT time = 10 min and temp = 622 °C; (e) SEM image for phototherma rapid growth process (PT-RGP); HT time ≈2.5 min and temp =659 °C. Total process time for PT-RGP is 3 min and 35 s. Scale bar for (a-e) is same. (f) In the plot, black lines represent temperature profiles for the conditions: HT = 10 min, Temp = 622 °C, and red lines represent the profiles for PT-RGP.

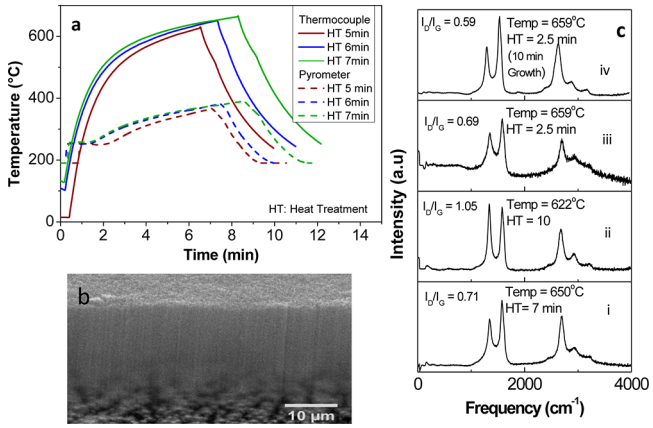

Figure 4. (a) Temperature profiles recorded by the pyrometer at the bottom (dashed lines) and thermocouple (solid lines) at the top surface of the samples. The Temperatures at the top surface of the samples after 5, 6, and 7 min HT times are 606, 634, and 651 °C, respectively (brown, blue and green solid lines). (b) SEM image of CNT grown sample where HT time ≈2.5 min and Growth time = 10 min. (c) Raman spectra of as-grown CNTs for 1 min growth after: (i) 7 min HT (Temp = 651 °C), (ii) 10 min HT (Temp = 622 °C) and (iii) 2.5 min HT (Temp = 659 °C). (iv) Raman spectrum corresponding to 2.5 min HT and 10 min CNT growth process.

catalyst HT using a PTCVD system.[16] They introduced H_2/C_2H_2 (100/6 sccm) simultaneously into the chamber at 2 Torr pressure and carried out growth for 15 min. However, the immediate start of the CNT growth had not been necessarily demonstrated. The CNT growth would have started after some time, as is observed in this study, with the CNT growth for 5 min HT and 3 min growth, which in fact, is equivalent to the 7 min HT and 1 min growth process. Therefore, unless an accurate understanding of the catalyst heat-treatment and CNT growth mechanism is established, predetermined, and controlled growth will not be possible.

The temperature values at the top surface of the samples after 5, 6, and 7 min HT are 606, 634 and 651 °C, respectively, Figure 4a. Here, there can be two possibilities in terms of HT time and temperature: (1) the CNT growth can occur at lower temperatures if HT time is >7 min. (2) the growth can occur at HT time <7 min if the temperature is higher than 651 °C. Interestingly, CNT growth is observed for both conditions. Selecting a lower electrical power (35%) supplied to the lamps, the surface temperature of the sample was controlled (black line in Figure 3f) at 622 °C (<650 °C), HT time was given 10 min (>7 min) and growth was carried out for 1 min. The SEM micrograph (Figure 3d) for this process shows shorter CNTs as compared with Figure 3c, indicating lower CNT growth rate for lower temperatures.[29]

As the temperature in the PTCVD system depends critically on the flow rates of gases and pressure inside the chamber,[34] we utilized this attribute of the system to confirm our second assumption. We turned the lamps on at 40% power under vacuum (1.6×10^{-5} Torr) with no gases flowing through the chamber. This allowed the surface temperature of the sample to increase rapidly reaching at 659 °C in just 2 min and 35 s (red line Figure 3f). After this, H_2 was introduced, the pressure was controlled at 2 Torr and then C_2H_2 was introduced for 1 min. The SEM image of the CNTs grown for this process is shown in Figure 3e. The as-grown CNTs are very similar to those in Figure 3(c), with lengths in excess of a micrometer. We have named this process as "photothermal rapid growth process" (PT-RGP) because, to the best of our knowledge, the total process time (HT and growth) is the shortest (less than 4 min) ever reported for the growth of CNTs on metallic layers with length >1 μm. Beside the ability of rapid temperature rising, the chamber cooling down process in PTCVD is also incredibly fast, compared with conventional hot wall CVD systems. Figure 4(b) shows the SEM image of the CNTs grown using the PT-RGP where the growth time is prolonged to 10 min. The CNTs are vertically aligned, dense ($\sim 1 \times 10^9$ cm^{-2}) and about 35 μm long, similar to those in Figure 1e. The total process time in this case is under 13 min. The advantages of the PT-RGP includes: reduced process time, reduced time that the sample spends at elevated temperatures thereby reducing thermal strain, reduced power and gases consumption and consequently reduced cost for CNT growth. These attributes make PT-RGP viable for interconnect applications.

The above evidence is an example of activating CNT growth at shorter HT times, using a high gradient to reach at a certain threshold value of the temperature (650 °C in this case). The mechanism of CNT growth in CVD can be considered in two stages: (1) catalyst pretreatment for the formation of active nanoparticles and (2) decomposition and nucleation of carbonaceous gas on catalyst particles. Since CNT growth for 10 min HT at a lower temperature (622 °C) is observed (Figure 3d), this implies that the growth is not hindered because of low temperatures as in the case of 5 and 6 min HT processes (Figure 3a, b), rather it is due to the shorter HT times. By contrast, PT-RGP (Figure 3e) suggests that the active-catalyst-particle formation process is quick enough above a certain threshold point (650 °C in this study) to initiate CNT

growth readily. Therefore, in our view, it is the formation of the active catalyst particles that determines the CNT growth initiation point and can be controlled by the HT temperature and duration. For lower temperatures (<650 °C), the formation process of active catalyst particles might be slow, and therefore, increased HT time is needed and vice versa. This explanation is also supported by the SEM image analysis in Figure 3a, where only few catalyst particles are observed as compared with Figure 3b.

The Raman spectra of as-grown CNTs for different HT times and temperatures are given in Figure 4c. The low I_D/I_G ratios of 0.71 and 0.69 (Figure 4c(i, iii)) for CNTs grown for 7 min HT process and PT-RGP respectively, indicate their similar high structural quality, whereas the CNTs for 10 min HT process at lower temperature resulted in higher I_D/I_G value of 1.05 (Figure 4c(ii)), indicating relatively more structural defects. The shorter length and decreased quality of the CNTs is attributed to the decreased growth temperature. The I_D/I_G value of 0.59 (Figure 4c(iv)) of CNTs grown for 10 min using PT-RGP is higher when compared with the I_D/I_G value (0.45) of CNTs grown after 10 min HT and 10 min growth (Figure 2c), indicating relatively lower graphitization in these structures. This difference is because of a sharp reduction in the temperature when relatively cold gases (H_2 and C_2H_2 at room temperature) were introduced into the chamber after annealing the sample for about 2.5 min in vacuum.

Finally, electrical characterization of the nanotube vias has been performed in which a 300 nm Ag layer was sputter-deposited over PT-RGP grown CNTs as a top metal contact. The bottom electrical layer is Ti/Cu/TiN and has a measured resistance of 0.27 Ω for an intervia separation of 1 mm. Electrical measurements were carried out by measuring the potential difference between two Ag-coated CNT-based vias for different separations for a given drive current, as shown schematically in (Figure 5a). Performing the measurements in this way eliminates the contact resistance between the probes and the silver top contact. A linear current−voltage relationship can be observed in Figure 5b. The calculated total resistance from the two vias and the bottom metal contact layer is 1.1 Ω and this results in the resistance of a single 100 × 100 μm^2 CNT to be 0.42 Ω. The corresponding via resistivity is about 4.2×10^{-3} Ω m. Our results are comparable with the transfer process placed CNTs of Fu et al.[35] and about 50% improved as compared with the recently published report by Dijon et al.[1]

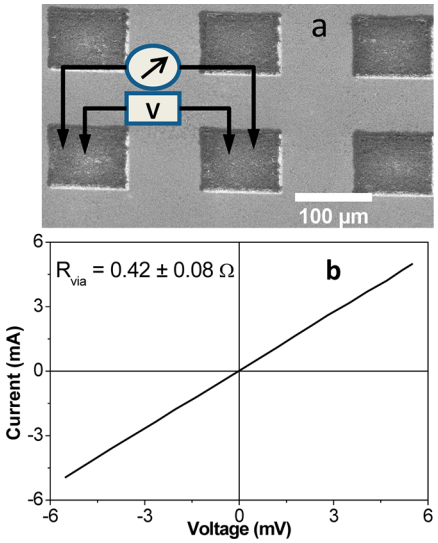

Figure 5. (a) Schematic of the electrical measurements with Ag coated CNT based vias. (b) Current−voltage relationship measured for two Ag-coated CNT-based vias having 1 mm separation between them. The resistance of a single Ag-coated CNT based via is calculated to be 0.42 Ω which is half of the difference between the total measured resistance and the resistance of the bottom contact metal.

CONCLUSIONS

High-quality catalyzed growth of CNTs using a PTCVD system at a substrate bulk temperatures below 415 °C has been achieved. The as-grown CNTs are vertically aligned, dense (~1×10^9 cm^{-2}) and growth occurred only in the predefined areas, where the catalyst was present. Furthermore, we have studied the effect of catalyst heat treatment time and temperature and found that increased heat treatment time is needed to initiate CNT growth for lower temperatures and vice versa. By rapidly reaching 659 °C at the top surface of the samples, the CNTs with lengths in excess of 1 μm were grown in less than 4 min of total process time (PT-RGP). The resistance of a single 100 × 100 μm^2 CNT-based via is calculated as 0.42 Ω, which is one of the best value reported for CNT-based via. Our results show that optically enhanced high-quality CNTs for interconnects can be grown rapidly at a CMOS-compatible temperature, using PTCVD. The broader impact of this work can be found in the possible application of the photothermal technology to other nanomaterial systems, such as graphene,[36] where catalyst activation is important.

METHODS

1. PTCVD Chamber Characteristics. The PTCVD chamber can be viewed in three parts: 1) an optical head, 2) the reaction chamber and 3) water-cooled chuck. In the optical head, eight equally spaced bulbs from GE lighting (model reference 88449-CP77 FEP 230-240 V) are installed in a 10 cm diameter circular geometry. The bulb diameter is 20 mm and length is 105 mm. The luminous flux at 100% efficiency of a single bulb is 25000 lm. At the back side of the array of lamps, there is a gold coated reflecting circular casing of 14 cm diameter. A quartz plate of 25 cm diameter present at the front of lamps isolates the whole optical head from the reaction chamber and allows the light transmission (in the visible and infrared region) into the reaction chamber. The reaction chamber is a 32 cm wide and 18 cm high metallic cylinder in which, the water-cooled chuck is present where a 4 in. wafer can be mounted. The distance between sample and optical head is 10 cm. The temperature at the top surface of the sample depends mainly on the electrical power supplied to the lamps, heat removal capacity of introduced gases and pressure of the chamber. The bulk temperature of the sample depends on the top and bottom temperature of the sample and on the thermal barrier layer used between catalyst and sample. No specific focusing is employed.

2. Catalyst Preparation. Figure 1a is the process schematic in which Ti/Cu/TiN (20/150/50 nm) layers were sputtered on n-Si substrates, where Ti and TiN films are used as diffusion barriers for Cu. Al (10 nm) was deposited over TiN film as an etch-stop and catalyst support material. After this, approximately 300 nm SiO_2 film was thermally grown, patterned lithographically, and etched (using buffered HF solution) to print 100 × 100 μm^2 squares, having 100 μm spacing between them. A 3 nm Fe layer to act as a catalyst was sputter-deposited and the photoresist was then removed.

3. Photothermal Chemical Vapor Deposition Process Parameters. The CNT growth on Ti/Cu/TiN patterned structure was conducted for 15 s to 20 min on different samples using a photothermal chemical vapor deposition (PTCVD) system.[16] This system utilizes the circulation of chilled water inside a cylindrical substrate holder to keep the substrate temperature low. An array of

optical lamps (1 kW each) at the head of the reaction chamber delivers the optical energy directly on the catalyst at the top surface of the sample. The temperature inside the chamber is controlled by the electrical power supplied to the optical lamps. A K-type thermocouple records the temperature at the top surface and an optical pyrometer present at the bottom, records the bulk temperature of the substrate.

Samples were preheated in 100 sccm (standard cubic centimeter per minute) H_2 flow for 10 min (including temperature ramping time) at 2 Torr pressure by applying 40% electrical power [100% power = 8 kW] to the optical lamps. After this, 10 sccm of C_2H_2 was introduced for 15 s to 20 min. Upon turning the lamps on, the temperature increases at a high rate, reaches at 323 °C bulk and 666 °C at the top surface of the sample in 10 min, then gradually becomes constant (Figure 1b). The bulk temperature of the samples remains below 415 °C for the entire growth series. The transmission of IR radiation through Si decreases as its temperature increases; initially the pyrometer (at the bottom side) reads all the signals reached to it (please see Figure 1b, the initial peak in the profile for pyrometer), however, after 250 °C it essentially records the nonlinearly averaged blackbody radiations emitted by the sample. There are mainly three reasons of the large temperature difference at the top and bottom of the sample: (i) the bottom side of the sample is in-contact with the water-cooled chuck, (ii) the metallic structure of Ti/Cu/TiN acts as a thermal barrier layer (TBL) between catalyst and Si substrate, which reflects the optical energy back to the catalyst and (iii) the H_2 flow at 2 Torr pressure efficiently removes the excess heat from the top surface of the sample and hence reduces the downward flow of heat.

4. Sample Characterization. The as-grown CNTs were characterized using an FEI quanta 200 scanning electron microscope (SEM), Renishaw Systems 2000 Raman Spectroscope using 514 nm laser wavelength, Philips CM 200 transmission electron microscope (TEM) and Keithley 4200 analyzer (for electrical measurements.

AUTHOR INFORMATION

Corresponding Author

*E-mail: s.silva@surrey.ac.uk.

Notes

The authors declare no competing financial interest.

ACKNOWLEDGMENTS

The authors acknowledge Surrey NanoSystems Ltd. for assisting us in our research activities.

REFERENCES

(1) Dijon, J.; Okuno, H.; Fayolle, M.; Vo, T.; Pontcharra, J.; Acquaviva, D.; Bouvet, D.; Ionescu, A. M.; Esconjauregui, C. S.; Capraro, B.; Quesnel, E.; Robertson, J. In *2010 International Electron Devices Meeting—Technical Digest*; IEEE: Piscataway, NJ, 2010.

(2) Srivastava, N.; Hong, L.; Kreupl, F.; Banerjee, K. *IEEE Trans. Nano.* **2009**, *8*, 542–559.

(3) Yokoyama, D.; Iwasaki, T.; Yoshida, T.; Kawarada, H.; Sato, S.; Hyakushima, T.; Nihei, M.; Awano, Y. *Appl. Phys. Lett.* **2007**, *91*, 3.

(4) Kawano, T.; Chung Yeung, C.; Liwei, L. In *2nd IEEE International Conference Nano/Micro Engineered and Molecular Systems (NEMS '07)*; Bangkok, Thailand, Jan 16–19, 2007 ; IEEE: Piscataway, NJ, 2007; pp 895–898.

(5) Connolly, T.; Smith, R. C.; Hernandez, Y.; Gun'ko, Y.; Coleman, J. N.; Carey, J. D. *Small* **2009**, *5*, 826–831.

(6) Zhang, Z.; Liang, X.; Wang, S.; Yao, K.; Hu, Y.; Zhu, Y.; Chen, Q.; Zhou, W.; Li, Y.; Yao, Y.; Zhang, J.; Peng, L.-M. *Nano Lett.* **2007**, *7*, 3603–3607.

(7) Yang, M. H.; Teo, K. B. K.; Milne, W. I.; Hasko, D. G. *Appl. Phys. Lett.* **2005**, *87*, 253116.

(8) International Technology Roadmap for Semiconductors, 2011 Edition: Interconnects. http://www.itrs.net/Links/2011ITRS/Home2011.htm

(9) Li, H. J.; Lu, W. G.; Li, J. J.; Bai, X. D.; Gu, C. Z. *Phys. Rev. Lett.* **2005**, *95*, 086601.

(10) Wei, B. Q.; Vajtai, R.; Ajayan, P. M. *Appl. Phys. Lett.* **2001**, *79*, 1172–1174.

(11) Pop, E.; Mann, D.; Wang, Q.; Goodson, K. E.; Dai, H. J. *Nano Lett.* **2006**, *6*, 96–100.

(12) Peng, B.; Locascio, M.; Zapol, P.; Li, S. Y.; Mielke, S. L.; Schatz, G. C.; Espinosa, H. D. *Nat. Nanotechnol.* **2008**, *3*, 626–631.

(13) Katagiri, M.; Sakuma, N.; Yamazaki, Y.; Suzuki, M.; Sato, S.; Nihei, M.; Sakai, T.; Awano, Y. *Jpn. J. Appl. Phys.* **2009**, *48*, 090205.

(14) Yokoyama, D.; Iwasaki, T.; Yoshida, T.; Kawarada, H.; Sato, S.; Hyakushima, T.; Nihei, M.; Awano, Y. *Appl. Phys. Lett.* **2007**, *91*, 263101.

(15) Kreupl, F.; Graham, A. P.; Duesberg, G. S.; Steinhogl, W.; Liebau, M.; Unger, E.; Honlein, W. *Microelectron. Eng.* **2002**, *64*, 399–408.

(16) Shang, N. G.; Tan, Y. Y.; Stolojan, V.; Papakonstantinou, P.; Silva, S. R. P. *Nanotechnology* **2010**, *21*, 505604.

(17) Lee, K. Y.; Honda, S. I.; Katayama, M.; Miyake, T.; Himuro, K.; Oura, K.; Lee, J. G.; Mori, H.; Hirao, T. *J. Vac. Sci. Tech. B* **2005**, *23*, 1450–1453.

(18) Dupuis, A. C. *Prog. Mater. Sci.* **2005**, *50*, 929–961.

(19) Chhowalla, M.; Teo, K. B. K.; Ducati, C.; Rupesinghe, N. L.; Amaratunga, G. A. J.; Ferrari, A. C.; Roy, D.; Robertson, J.; Milne, W. I. *J. Appl. Phys.* **2001**, *90*, 5308–5317.

(20) Mathur, A.; Roy, S. S.; Dickinson, C.; McLaughlin, J. A. *Curr. Appl. Phys.* **2010**, *10*, 407–410.

(21) Brown, S. D. M.; Jorio, A.; Dresselhaus, M. S.; Dresselhaus, G. *Phys. Rev. B* **2001**, *64*, 073403.

(22) Eklund, P. C.; Holden, J. M.; Jishi, R. A. *Carbon* **1995**, *33*, 959–972.

(23) Tuinstra, F.; Koenig, J. L. *J. Chem. Phys.* **1970**, *53*, 1126–1130.

(24) Saito, R.; Gruneis, A.; Samsonidze, G. G.; Brar, V. W.; Dresselhaus, G.; Dresselhaus, M. S.; Jorio, A.; Cancado, L. G.; Fantini, C.; Pimenta, M. A.; Souza, A. G. *New J. Phys.* **2003**, *5*, 157.

(25) Wang, Y.; Alsmeyer, D. C.; McCreery, R. L. *Chem. Mater.* **1990**, *2*, 557–563.

(26) Campos-Delgado, J.; Kim, Y. A.; Hayashi, T.; Morelos-Gomez, A.; Hofmann, M.; Muramatsu, H.; Endo, M.; Terrones, H.; Shull, R. D.; Dresselhaus, M. S.; Terrones, M. *Chem. Phys. Lett.* **2009**, *469*, 177–182.

(27) Bagiante, S.; Scalese, S.; Scuderi, V.; D'Urso, L.; Messina, E.; Compagnini, G.; Privitera, V. *Phys. Stat. Solidi B* **2010**, *247*, 884–887.

(28) Babanejad, S. A.; Malekfar, R.; Hosseini, S. M. R. S. *Acta Phys. Pol., A* **2009**, *116*, 217–220.

(29) Lee, Y. T.; Park, J.; Choi, Y. S.; Ryu, H.; Lee, H. J. C. *J. Phys. Chem. B* **2002**, *106*, 7614–7618.

(30) Lee, C. J.; Park, J.; Huh, Y.; Lee, J. Y. *Chem. Phys. Lett.* **2001**, *343*, 33–38.

(31) Mizuno, K.; Ishii, J.; Kishida, H.; Hayamizu, Y.; Yasuda, S.; Futaba, D. N.; Yumura, M.; Hata, K. *Proc. Natl. Acad. Sci. U.S.A.* **2009**, *106*, 6044–6047.

(32) Daniels, H.; Brydson, R.; Rand, B.; Brown, A. *Philos. Mag.* **2007**, *87*, 4073–4092.

(33) Seidel, R.; Duesberg, G. S.; Unger, E.; Graham, A. P.; Liebau, M.; Kreupl, F. *J. Phys. Chem. B* **2004**, *108*, 1888–1893.

(34) Chen, G. Y.; Jensen, B.; Stolojan, V.; Silva, S. R. P. *Carbon* **2011**, *49*, 280–285.

(35) Fu, Y. F.; Qin, Y. H.; Wang, T.; Chen, S.; Liu, J. H. *Adv. Mater.* **2010**, *22*, 5039.

(36) Tan, Y. Y.; Jayawardena, K. D. G. I.; Adikaari, A. A. D. T.; Tan, L. W.; Anguita, J. V.; Henley, S. J.; Stolojan, V.; Carey, J. D.; Silva, S. R. P. *Carbon* **2012**, *50*, 668–673.